

Hydrogen sulphide at high pressure: a strongly-anharmonic phonon-mediated superconductor

Ion Errea^{1,2}, Matteo Calandra^{3,*}, Chris J. Pickard⁴, Joseph Nelson⁵, Richard J. Needs⁵, Yinwei Li⁶, Hanyu Liu⁷, Yunwei Zhang⁸, Yanming Ma⁸, and Francesco Mauri²

¹*Donostia International Physics Center (DIPC), Manuel de Lardizabal pasealekua 4, 20018 Donostia-San Sebastián, Basque Country, Spain*

²*IKERBASQUE, Basque Foundation for Science, Bilbao, Spain*

³*IMPMC, UMR CNRS 7590, Sorbonne Universités - UPMC Univ. Paris 06, MNHN, IRD, 4 Place Jussieu, F-75005 Paris, France*

⁴*Department of Physics & Astronomy, University College London, Gower Street, London WC1E 6BT, UK*

⁵*Theory of Condensed Matter Group, Cavendish Laboratory, J J Thomson Avenue, Cambridge CB3 0HE, UK*

⁶*School of Physics and Electronic Engineering, Jiangsu Normal University, Xuzhou 221116, People's Republic of China*

⁷*Department of Physics and Engineering Physics, University of Saskatchewan, Saskatchewan S7N 5E2, Canada and*

⁸*State Key Laboratory of Superhard Materials, Jilin University, Changchun 130012, People's Republic of China*

(Dated: February 11, 2015)

We use first principles calculations to study structural, vibrational and superconducting properties of H₂S at pressures $P \geq 200$ GPa. The inclusion of zero point energy leads to two different possible dissociations of H₂S, namely $3\text{H}_2\text{S} \rightarrow 2\text{H}_3\text{S} + \text{S}$ and $5\text{H}_2\text{S} \rightarrow 3\text{H}_3\text{S} + \text{HS}_2$, where both H₃S and HS₂ are metallic. For H₃S, we perform non-perturbative calculations of anharmonic effects within the self-consistent harmonic approximation and show that the harmonic approximation strongly overestimates the electron-phonon interaction ($\lambda \approx 2.64$ at 200 GPa) and T_c . Anharmonicity hardens H–S bond-stretching modes and softens H–S bond-bending modes. As a result, the electron-phonon coupling is suppressed by 30% ($\lambda \approx 1.84$ at 200 GPa). Moreover, while at the harmonic level T_c decreases with increasing pressure, the inclusion of anharmonicity leads to a T_c that is almost independent of pressure. High pressure hydrogen sulfide is a strongly anharmonic superconductor.

Cuprates [1] have for many years held the world record for the highest superconducting critical temperature ($T_c = 133$ K) [2]. However, despite almost 30 years of intensive research, the physical mechanism responsible for such a high T_c is still elusive, although the general consensus is that it is highly non-conventional. The discovery by Drozdov *et al.* [3] of $T_c = 190$ K in a diamond anvil cell loaded with hydrogen sulfide (H₂S) and compressed to about 200 GPa breaks the cuprates record and overturns the conventional wisdom that such a high T_c cannot be obtained via phonon-mediated pairing.

The claim that hydrogen at high pressure could be superconducting is not new [4] and it was recently supported by first principles calculations based on the harmonic approximation applied to dense hydrogen [5–8] and several hydrides [9–15]. More recently, two theoretical papers predicted the occurrence of high T_c superconductivity in high-pressure sulfur-hydrides [16, 17]. However, as shown in Refs. [18, 19], anharmonicity can be crucial in these systems. For example, in PdH, the electron-phonon coupling λ parameter is found to be 1.55 at the harmonic level, while a proper inclusion of anharmonic effects leads to $\lambda = 0.40$ [18], in better agreement with experiments. Thus, in hydrogen-based compounds, the phonon spectra are strongly affected by anharmonic effects.

Several first principles calculations [16, 17, 20, 26] suggested that decomposition of the H₂S sample occurs

within the diamond-anvil cell at high pressures. The high- T_c superconducting material is therefore very unlikely to be H₂S, while H₃S is the obvious candidate for the H-rich decomposition product.

Here we study the structural, vibrational and superconducting properties of H₂S above 200 GPa, where the highest T_c occurs. We show that the inclusion of zero point motion in the convex hull at 200 and 250 GPa stabilizes two metallic structures, H₃S and HS₂. Finally, we show that, contrary to suggestions in previous work [16, 20], the harmonic approximation does not explain the measured T_c in H₃S, and the inclusion of anharmonic effects is crucial.

As decomposition of H₂S has been demonstrated in the experiments of Ref. [3], it is crucial to develop an understanding of the different H/S compounds that might be stable in the pressure range of interest. We therefore perform a search over 43 H/S stoichiometries, determining the stoichiometries at which stable structures exist, and the associated crystal structures. These searches were performed using the *ab initio* random structure searching (AIRSS) method [21, 22] and the CALYPSO particle swarm optimization method of Ref. [23]. More information about the searches is provided in the Supplemental Material [24].

The results of the structure searching are shown in Fig. 1. At 200 GPa, without zero-point energy (ZPE), the only energetically allowed decomposition is $3\text{H}_2\text{S} \rightarrow 2\text{H}_3\text{S}$

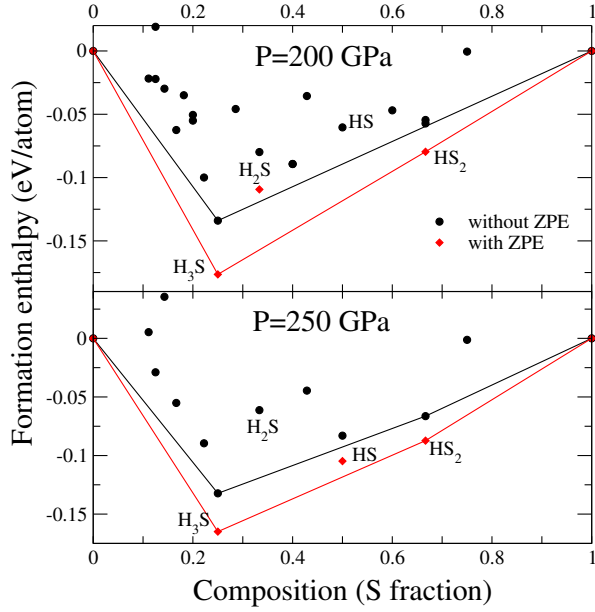


FIG. 1. Results of structure searching at 200 and 250 GPa. Convex hulls are shown as continuous lines, with and without the inclusion of zero point energy (ZPE).

+ S, in agreement with previous calculations [16, 20, 25, 26]. H_3S crystallizes in the space group $Im\bar{3}m$, as shown in [16]. When ZPE is included, a second decomposition becomes possible at 200 GPa, namely $5\text{H}_2\text{S} \rightarrow 3\text{H}_3\text{S} + \text{HS}_2$, where HS_2 crystallizes in a structure of space group $C2/c$ with 12 atoms/cell. At 250 GPa and above, the latter decomposition is allowed even without ZPE, and the $C2/c$ HS_2 structure undergoes a phase transition to a more stable $C2/m$ structure with 6 atoms/cell. Each of the HS_2 structures is metallic. Finally, at 300 GPa, an HS phase becomes stable [24]. Detailed information on the crystal structures is provided in the Supplemental Material [24].

Having determined the most stable crystal structures at high pressure, we turn to the study of vibrational properties [27, 28]. We consider the $Im\bar{3}m$ H_3S structure at 200 GPa [33]. In this structure each H atom is twofold coordinated and has 6 neighbors, 2 of which are S atoms while the other 4 are H atoms. H vibrations can then be decomposed into HS bond-stretching modes (H_{\parallel}), in which an H atom moves towards one of the two S atoms, and bond-bending modes (H_{\perp}), in which one H atom moves in the direction perpendicular to the H-S bond (see Fig. 1 in [24]). The harmonic phonon spectrum of H_3S is shown in Fig. 2 and overall shows a clear separation into H modes at high energy and S modes below 75 meV. To gain more insight we use Wannier interpolation [31, 32] of the electron-phonon matrix elements and evaluate the electron-phonon contribution to the phonon

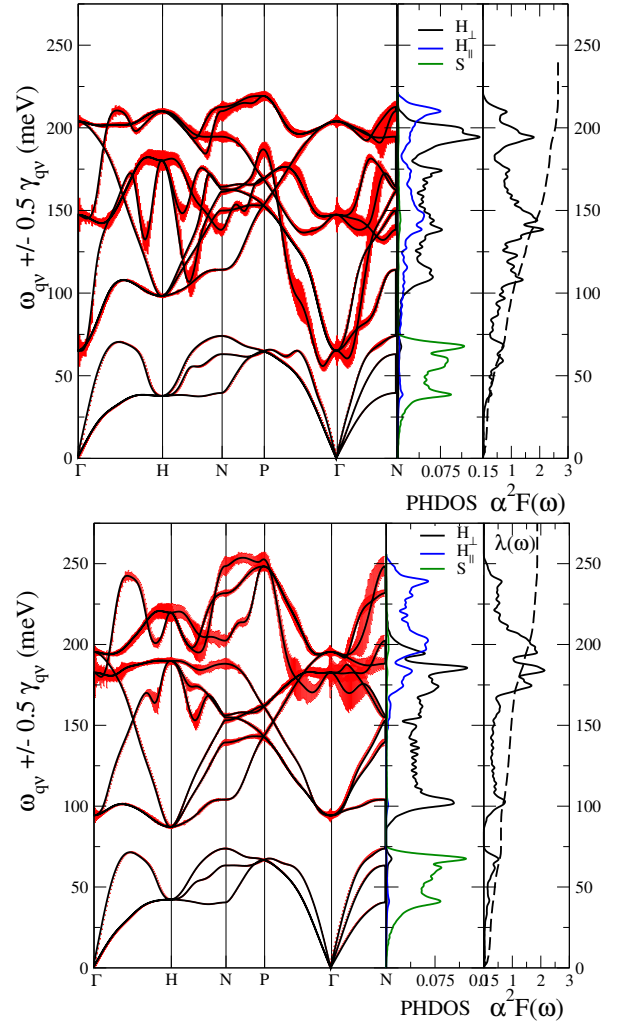


FIG. 2. Phonon dispersion, phonon density of states projected onto selected atoms and directions, and the Eliashberg function of H_3S in the harmonic approximation (top) and with the inclusion of anharmonic effects (bottom) for H_3S at 200 GPa. H_{\perp} and H_{\parallel} label displacements of an H atom in the directions perpendicular or parallel to a H-S bond. The magnitude of the phonon linewidth is indicated by the size of the red error bars.

linewidth, as [34]:

$$\gamma_{\mathbf{q}\nu} = \frac{4\pi\omega_{\mathbf{q}\nu}}{N_k} \sum_{\mathbf{k}, n, m} |g_{nm}^{\nu}(\mathbf{k}, \mathbf{k} + \mathbf{q})|^2 \delta(\varepsilon_{\mathbf{k}n}) \delta(\varepsilon_{\mathbf{k}+\mathbf{q}m}). \quad (1)$$

Here $\omega_{\mathbf{q}\nu}$ are the phonon frequencies, N_k the number of electron-momentum points in the grid, $g_{nm}^{\nu}(\mathbf{k}, \mathbf{k} + \mathbf{q}) = \langle \mathbf{k}n | \delta V_{KS} / \delta u_{\mathbf{q}\nu} | \mathbf{k} + \mathbf{q}m \rangle$ is the electron-phonon matrix element, V_{KS} is the Kohn-Sham potential, and $u_{\mathbf{q}\nu}$ is a phonon displacement. The Kohn-Sham energy and eigenfunctions are labeled $\varepsilon_{\mathbf{k}n}$ and $|\mathbf{k}n\rangle$. The electron-phonon coupling at a given phonon-momentum \mathbf{q} for a phonon mode ν can be obtained [34] from the phonon linewidth as $\lambda_{\mathbf{q}\nu} = \frac{\gamma_{\mathbf{q}\nu}}{2\pi\omega_{\mathbf{q}\nu}^2 N(0)}$.

As shown in Fig. 2, at the harmonic level, the phonon linewidths of the H vibrations is fairly uniform throughout the spectrum. The contribution of each mode to the average electron-phonon interaction, $\lambda = \sum_{\mathbf{q}\nu} \lambda_{\mathbf{q}\nu}/N_q$, can be obtained from the isotropic Eliashberg function

$$\alpha^2 F(\omega) = \frac{1}{2N_q} \sum_{\mathbf{q}\nu} \lambda_{\mathbf{q}\nu} \omega_{\mathbf{q}\nu} \delta(\omega - \omega_{\mathbf{q}\nu}) \quad (2)$$

where N_q is the number of phonon-momentum points in the grid. $\lambda(\omega) = 2 \int_0^\omega \frac{\alpha^2 F(\omega')}{\omega'} d\omega'$ and then $\lambda = \lambda(\infty)$. We find $\lambda = 2.64$ (see Table IV), which is larger than that obtained in Refs. [16, 20, 26] with a much coarser sampling of the BZ. This huge value of λ comprises substantial contributions from many H vibrational modes. The situation is therefore very different from MgB_2 in which a single mode dominates λ .

Given the low mass of H and the consequent large phonon displacements, we investigate the occurrence of anharmonic effects using the stochastic self-consistent harmonic approximation (SSCHA) developed by some of us [18, 19, 35]. As shown in Fig. 2 (bottom), the anharmonic correction leads to non-trivial changes in the harmonic spectrum. While it is very clear that all H bond-stretching modes are hardened, the effect on H bond-bending modes is less straightforward. By computing the average phonon frequency as of H_{\parallel} and of H_{\perp} modes we find that $\bar{\omega}_{\parallel}^{\text{har}} \approx 158.1$ meV and $\bar{\omega}_{\parallel}^{\text{anh}} \approx 203.3$ meV, while for bond-bending modes $\bar{\omega}_{\perp}^{\text{har}} \approx 157.0$ meV and $\bar{\omega}_{\perp}^{\text{anh}} \approx 147.9$ meV. Thus bond-stretching modes are hardened, while bond-bending modes are softened.

It is important to remark that the large and most dispersive mode along PF is strongly hardened at the anharmonic level and undergoes a non-trivial change in polarization, as can be seen from the large effect of anharmonicity on the phonon linewidth $\gamma_{\mathbf{q}\nu}$ in Fig. 2. It is worthwhile to recall that the phonon-linewidth depends on the phonon eigenvector but not on the phonon energy. This effect demonstrates the need to calculate not only the phonon frequencies at the anharmonic level, but also the phonon polarizations.

The anharmonic electron-phonon interaction is $\lambda = 1.84$, which is 30% smaller than the harmonic result. This reduction is mostly explained by the hardening of the H_{\parallel} modes. In contrast to the harmonic case which shows uniform coupling over all modes, the anharmonic Eliashberg function has two main peaks, a broad peak in the 40–75 meV region, and a second one in the 175–200 meV region. Their contributions to λ are 0.59 and 0.77, respectively, accounting for $\approx 73\%$ of the total λ . We note, however, that the logarithmic average of the phonon frequencies, ω_{\log} , is only weakly enhanced by anharmonicity (see Table IV).

The superconducting critical temperature can be obtained either from the McMillan equation or the isotropic Migdal-Eliashberg approach. However, it is well known

[36] that the use of the McMillan equation for such values of λ leads to a substantial underestimation of T_c . We solved the isotropic Eliashberg equations [24] and found, contrary to claims in previous publications [16, 20], that calculations based on the harmonic phonon spectrum do not explain the measured T_c as, even using large values of μ^* [37, 38], T_c is substantially overestimated (i.e., $T_c = 250$ K for $\mu^* = 0.16$ [24]). When the anharmonic phonon spectrum and electron-phonon coupling are used, the Migdal-Eliashberg equations account for the experimental T_c when the value $\mu^* = 0.16$ is used, as shown in Table IV. The superconducting gap at zero temperature is $\Delta \approx 36.5$ meV.

Interestingly, the large anharmonic effects lead to very different variation of T_c with pressure. By repeating the calculation for the $Im\bar{3}m$ structure at 250 GPa, we found at the harmonic level and using the Migdal-Eliashberg equations with the same values of $\mu^* = 0.16$, that $T_c = 226$ K, decreasing with increasing pressure. However, at the anharmonic level we find $T_c = 190$ K, essentially independent of pressure in the region 200–250 GPa.

Finally, we consider the extent to which the occurrence of large anharmonic effects can explain the isotope shift in D_2S . At 164 GPa, $T_c(\text{D}_2\text{S}) = 90$ K, leading to an isotope coefficient $\alpha \approx 1.07$, which is substantially enhanced from the canonical BCS value of $\alpha \approx 0.5$. Assuming a similar decomposition of D_2S into D_3S and S at high pressures, we calculate the anharmonic phonon spectrum (see [24]) and electron-phonon coupling in D_3S at 200 GPa. We find at the anharmonic level that the electron-phonon coupling is essentially unaffected, while ω_{\log} is softened from 92.9 meV to 73.3 meV, leading to an isotope coefficient of $\alpha = 0.35$, which is strongly reduced from the BCS value but inconsistent with the value of $\alpha \approx 1.07$ found in experiments. Thus, contrary of what claimed in Ref. 39, anharmonicity reduces α .

TABLE I. Electron-phonon interaction and logarithmic averages of phonon frequencies, with and without anharmonic effects. The T_c s are calculated using the isotropic Migdal-Eliashberg equations (T_c^{ME}). A value of $\mu^* = 0.16$ is used. Data for T_c calculated with the McMillan equation is provided in the Supplemental Material [24]. Frequencies are in meV and T_c s are in K.

Compound	λ^{har}	$\omega_{\log}^{\text{har}}$	λ^{anh}	$\omega_{\log}^{\text{anh}}$	$T_c^{\text{ME,har}}$	$T_c^{\text{ME,anh}}$	$T_c(\text{Exp})$
H_3S (200 GPa)	2.64	90.4	1.84	92.86	250	194.0	190
H_3S (250 GPa)	1.96	109.1	1.71	101.3	226	190	
D_3S (200 GPa)	2.64	68.5	1.87	73.3	183	152.0	90

We have studied the structural, vibrational and superconducting properties of high pressure H_3S . We have included zero point motion when comparing the stabilities of different H/S phases, which has been neglected in other publications so far. This is important because zero point motion stabilises a new phase at $P \geq 200$ GPa. In particular, we found that decomposition of HS_2 into metallic phases can occur following two main paths, namely $3\text{H}_2\text{S}$

$\rightarrow 2\text{H}_3\text{S} + \text{S}$ and $5\text{H}_2\text{S} \rightarrow 3\text{H}_3\text{S} + \text{HS}_2$. We have performed a detailed study of the vibrational properties of high pressure H_3S and D_3S , finding that the phonon spectra are strongly affected by anharmonic effects. Anharmonicity hardens H–S bond-stretching modes and softens H–S bond-bending modes. Moreover, anharmonicity leads to a reduction in the electron-phonon coupling by $\approx 30\%$ and to an approximately constant T_c in the range 200–250 GPa. Our work demonstrates that the superconducting properties of high pressure H_3S can only be properly described by including both nuclear quantum effects and anharmonicity.

We acknowledge discussions with I. I. Mazin and support from the Graphene Flagship and Agence nationale de la Recherche, grant n. ANR-13-IS10-0003-01. Computer facilities were provided by PRACE, CINES, CCRT and IDRIS. I.E. acknowledges financial support from the Department of Education, Language Policy and Culture of the Basque Government (Grant No. BFI-2011-65) and the Spanish Ministry of Economy and Competitiveness (FIS2013-48286-C2-2-P). C.J.P. and R.J.N. thank EPSRC (UK) for financial support. J.R.N. acknowledges financial support from the Cambridge Commonwealth Trust. Y. Li thanks the National Natural Science Foundation of China under Grant Nos. 11204111 and 11404148. Y. Zhang and Y. Ma thank the Natural Science Foundation of China under No. 11274136, the 2012 Changjiang Scholars Program of China.

* matteo.calandra@upmc.fr

- [1] J. G. Bednorz and K. A. Mueller, *Zeitschrift für Physik B* **64** 189, (1986).
- [2] A. Schilling, M. Cantoni, J. D. Guo, and H. R. Ott, *Nature* **363**, 56 (1993).
- [3] A. P. Drozdov, M. I. Eremets, I. A. Troyan, arXiv:1412.0460 (unpublished).
- [4] N. W. Ashcroft, *Phys. Rev. Lett.* **21**, 1748 (1968).
- [5] Lijun Zhang, Yingli Niu, Quan Li, Tian Cui, Yi Wang, Yanming Ma, Zhi He, Guangtian Zou, *Solid State Communications*, **141**, 610 (2007).
- [6] P. Cudazzo, G. Profeta, A. Sanna, A. Floris, A. Continenza, S. Massidda, and E. K. U. Gross, *Phys. Rev. Lett.* **100**, 257001 (2008).
- [7] P. Cudazzo, G. Profeta, A. Sanna, A. Floris, A. Continenza, S. Massidda, and E. K. U. Gross, *Phys. Rev. B* **81**, 134505 (2010).
- [8] P. Cudazzo, G. Profeta, A. Sanna, A. Floris, A. Continenza, S. Massidda, and E. K. U. Gross, *Phys. Rev. B* **81**, 134506 (2010).
- [9] D. Y. Kim, R. H. Scheicher, C. J. Pickard, R. J. Needs, and R. Ahuja, *Phys. Rev. Lett.* **107**, 117002 (2011).
- [10] T. Scheler, O. Degtyareva, M. Marques, C. L. Guillaume, J. E. Proctor, S. Evans, and E. Gregoryanz, *Phys. Rev. B* **83**, 214106 (2011).
- [11] X.-F. Zhou, A. R. Oganov, X. Dong, L. Zhang, Y. Tian, and H.-T. Wang, *Phys. Rev. B* **84**, 054543 (2011).
- [12] Duck Young Kim, Ralph H. Scheicher, Ho-kwang Mao, Tae W. Kang, and Rajeev Ahuja, *Proc. Natl. Acad. Sci. USA* **107**, 2793 (2010).
- [13] Guoying Gao, Artem R. Oganov, Peifang Li, Zhenwei Li, Hui Wang, Tian Cui, Yanming Ma, Aitor Bergara, Andriy O. Lyakhov, Toshiaki Iitaka, and Guangtian Zou, *Proc. Natl. Acad. Sci. USA* **107**, 1317 (2010).
- [14] Guoying Gao, Artem R. Oganov, Aitor Bergara, Miguel Martinez-Canales, Tian Cui, Toshiaki Iitaka, Yanming Ma, and Guangtian Zou, *Phys. Rev. Lett.* **101**, 107002 (2008).
- [15] J. Feng, W. Grochala, T. Jaron, R. Hoffman, A. Bergara, and N. W. Ashcroft, *Phys. Rev. Lett.* **96**, 017006 (2006).
- [16] Defang Duan, Yunxian Liu, Fubo Tian, Da Li, Xi- aoli Huang, Zhonglong Zhao, Hongyu Yu, Bingbing Liu, Wenjing Tian, Tian Cui, *Sci. Rep.* **4**, 6968 (2014).
- [17] Yinwei Li, Jian Hao, Hanyu Liu, Yanling Li, and Yanming Ma *The J. of Chem. Phys.* **140**, 174712 (2014).
- [18] I. Errea, M. Calandra and F. Mauri, *Phys. Rev. Lett.* **111**, 177002 (2013).
- [19] Ion Errea, Matteo Calandra, and Francesco Mauri, *Phys. Rev. B* **89**, 064302 (2014).
- [20] J. A. Flores-Livas, A. Sanna, and E. K. U. Gross, arXiv:1501.06336
- [21] C. J. Pickard and R. J. Needs, *Phys. Rev. Lett.* **97**, 045504 (2006).
- [22] C. J. Pickard and R. J. Needs, *J. Phys.: Condensed Matter* **23**, 053201 (2011).
- [23] Wang, Lv, Zhu, and Ma, *Comput. Phys. Commun.* **183**, 2063 (2012).
- [24] See supplementary material at... for convex hull of H_3S at 300 GPa, effect of the zero point energy on the convex hull at 200 GPa, crystal structures, electronic structure of H_3S , vibrational properties of D_3S at 200 GPa and H_3S at 250 GPa, solution of Migdal-Eliashberg equations, effects of the vibrational zero point energy on pressure.
- [25] N. Bernstein, C. S. Hellberg, M. D. Johannes, I. I. Mazin, and M. J. Mehl, arXiv:1501.00196 (unpublished).
- [26] R. Akashi, M. Kawamura, S. Tsuneyuki, Y. Nomura, and R. Arita, arXiv:1502.00936
- [27] P. Giannozzi *et al.*, *J. Phys. Condens. Matter* **21**, 395502 (2009).
- [28] Our results were obtained from first-principles DFT linear-response calculations as implemented in the QUANTUM-ESPRESSO [27] package. We used ultrasoft [29] pseudopotentials, a generalized gradient approximation [1], a plane-wave cutoff energy of 60 Ry on the kinetic energy and 600 Ry on the charge density. The charge density and dynamical matrices were calculated using a 32^3 Monkhorst-Pack shifted electron-momentum grid and an Hermitian-Gaussian smearing of 0.03 Ry. The average electron-phonon coupling was obtained using Wannier interpolation [31]. We used a 32^3 electron-momentum grid randomly shifted from the origin and a 32^3 Monkhorst-Pack shifted phonon-momentum grid with a smearing of 0.03 eV. The phonon linewidth at a given phonon momentum was calculated using a $50 \times 50 \times 50$ electron-momentum mesh (randomly shifted from the origin).
- [29] D. Vanderbilt, *Phys. Rev. B* **41**, 7892 (1990).
- [30] J. P. Perdew, K. Burke, M. Ernzerhof, *Phys. Rev. Lett.* **77**, 3865 (1996).
- [31] M. Calandra, G. Profeta, and F. Mauri, *Phys. Rev. B* **82**, 165111 (2010).
- [32] F. Giustino, J. R. Yates, I. Souza, M. L. Cohen, and S.

- G. Louie, Phys. Rev. Lett. **98**, 047005 (2007).
- [33] The pressure computed here is without inclusion of ZPE. Neglecting ZPE underestimates the pressure of ≈ 12 GPa for H₃S and 6 GPa for D₃D for a volume of 89.9822 (a.u.)³. See [24] for more details.
- [34] P. B. Allen, Phys. Rev. B **6**, 2577 (1972), P. B. Allen and R. Silbergliitt, Phys. Rev. B **9**, 4733 (1974).
- [35] The SSCHA calculations were performed using a 3x3x3 supercell for both H₃S and D₃S at 0 K, yielding dynamical matrices on a commensurate 3x3x3 q -point grid. An additional calculation at 200 K conformed that temperatures within the range of the predicted superconductivity does not affect the phonon spectra. The difference between the harmonic and anharmonic dynamical matrices in the 3x3x3 phonon momentum grid was interpolated to a 6x6x6 grid. Adding the harmonic matrices to the result, the anharmonic dynamical matrices were obtained in a 6x6x6 grid. These dynamical matrices were used for the anharmonic electron-phonon coupling calculation.
- [36] P. B. Allen and R. C. Dynes, Phys. Rev. B **12**, 905 (1975).
- [37] P. Morel and P. W. Anderson, Phys. Rev. **125**, 1263 (1962).
- [38] N. N. Bogoliubov, V. V. Tolmachev, and D. V. Shirkov, *A New Method in the Theory of Superconductivity* (1958) (translation: Consultants Bureau, Inc., New York, 1959).
- [39] D. A. Papaconstantopoulos, B. M. Klein, M. J. Mehl, and W. E. Pickett, arXiv:1501.03950v1

Supplementary Materials of
Hydrogen Sulfides at high-pressure: a strongly-anharmonic phonon-mediated superconductor.

Technical details for the structural searching

We use the CALYPSO and AIRSS codes. Structure searching were performed at 200, 250, and 300 GPa for several H-S compounds (H8S, H7S, H6S, H5S, H4S, H3S, H2S, HS, H3S2, H2S3, H5S2, H9S2, HS2, H4S3, HS3, H3S2, H7S2) with maximum eight formula unit in the models. Each generation contained 40 structures, and the first generation was produced randomly with symmetry constraint. All structures were locally optimized using density functional theory with the Perdew-Burke-Ernzerhof (PBE) [1]. generalized gradient approximation implemented in the Vienna ab initio simulation package[2, 3]. An energy cutoff of 700 eV and a Monkhorst-Pack Brillouin zone sampling grid with a resolution of 0.5 \AA^{-1} were used in structure searches. The 60% lowest-enthalpy structures of each generation were used to produce the structures in the next generation by local PSO technique, and the remaining 40% structures were randomly generated within symmetry constraint to enhance the structural diversity. Typically, the structure searching simulation for each composition was stopped when 1000 successive structures were generated after a lowest energy structure was found. A number of distinct low-enthalpy structures found were then re-optimized with denser grids better than 0.2 \AA^{-1} and a higher energy cutoff of 1000 eV. The lowest-enthalpy structures were then chose to draw the convex-hull.

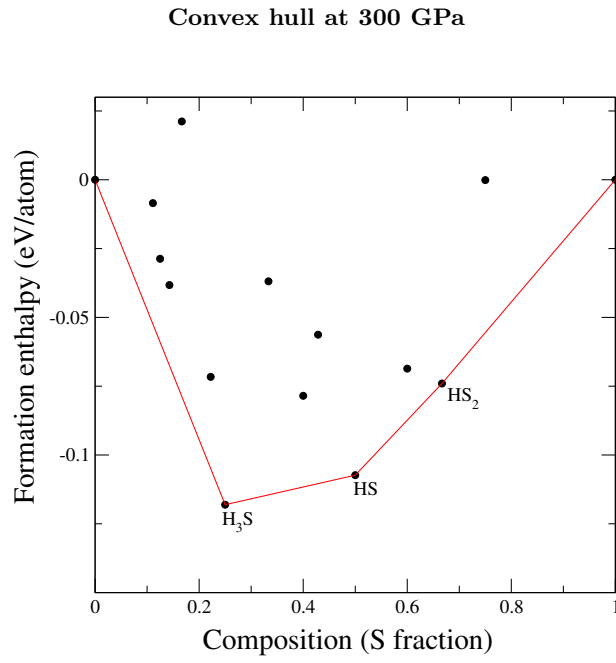


FIG. 3. Results of structural searches at 300 GPa. The continuous line shows the convex hull.

Effect of the zero point energy on the D_2S convex hull at 200 GPa

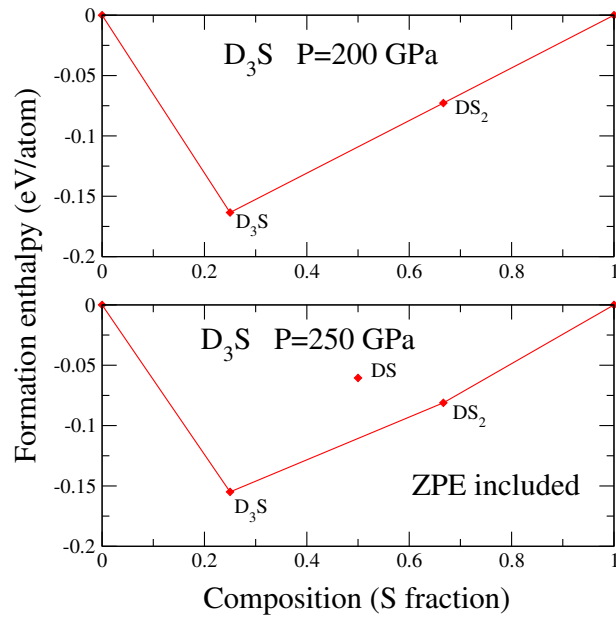


FIG. 4. Results of structural searches at 200 and 250 GPa for D-S structures including zero point energy. The continuous lines show the convex hull

Crystal structures for H and S

The crystal structure for Hydrogen is from Ref. [5]. The crystal structure for S is from Ref. [6]

Crystal structures of HS₂ at 200, 250 and 300 GPa

TABLE II. Crystallographic data for HS₂ at 200, 250 GPa as obtained from structural searches. At 250 and 300 GPa, HS₂ adopts the same C2/m structure as at 250 GPa.

Structure	Pressure (GPa)	Structural parameters (Å, deg.)	Atomic Positions			
C2/c	200	a=6.7827, b=4.1876, c=7.5401 $\alpha = 90, \beta = 137.7464, \gamma = 90$	S 8f	0.07702	0.12708	0.42711
			S 8f	0.89224	0.37399	0.79574
			H 8f	0.28345	0.86882	0.42463
C2/m	250	a=7.2073, b=2.947, c=3.6324, $\alpha = 90, \beta = 60.2287, \gamma = 90$	S 4i	0.33820	0.5	0.51566
			S 4i	0.59068	0.0	0.14405
			H 4i	0.61860	0.5	0.94147

The HS₂ crystal structures found with the CALYPSO and AIRSS codes are shown in Table III.

Crystal structures of HS and at 200, 250 and 300 GPa

TABLE III. Crystallographic data for HS at 200 and 300 GPa as obtained from structural searches. At 250 GPa and 300 GPa, HS₂ adopts the same C2/m structure.

Structure	Pressure	Structural parameters	Atomic Positions		
I4 ₁ /amd	200	a=b=2.9399, c=9.0531	S 16h	0.0	0.0 0.27894
			H 16h	0.5	0.0 0.62786
C2/m	300	a=9.4579, b=2.7388, c=2.749, $\alpha = 90, \beta = 73.1325, \gamma = 90$	S 4i	0.41556	0 0.83415
			S 4i	0.33437	0.5 0.41585
			H 4i	0.00217	0.0 0.24756
			H 4i	0.25205	0.5 0.99709

Crystal structure of H₃S at 200 and 250 GPa

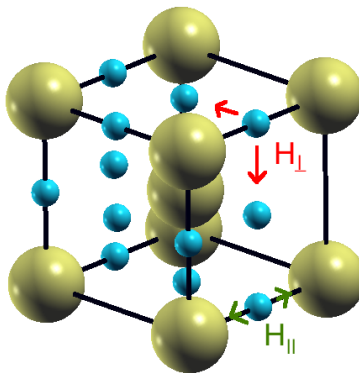


FIG. 5. Crystal structure of H₃S at 200 and 250 GPa. Hydrogen is depicted in cyan while sulfur is in yellow. The red (green) arrows label the H-S bond-bending (-stretching) modes, labeled H_⊥ (H_∥). The volumes at 200 and 250 are 13.3334 Å³, and 12.4925 Å³, respectively.

Electronic structure of H₃S at 200 GPa

The electronic structure of H₃S at 200 GPa is shown in Fig. 7 in the *fat-bands* representation including decomposition into H and S atomic states. In a 20 eV energy window around the Fermi level (ϵ_f), the electronic structure can be fairly well interpreted in terms of free electrons on a bcc lattice. However, in the proximity of the Fermi level, there is a substantial hybridization between the H and S electronic states, leading to avoided crossings at special points N, Γ and along the H-N high symmetry direction. The hybridization results in a peak in the density of states at approximately 0.17 eV below ϵ_f . At precisely ϵ_f , the density of states per spin is $N(0) = 0.33$ states/eV/spin/H₃S cell, which is essentially identical to the free-electron value.

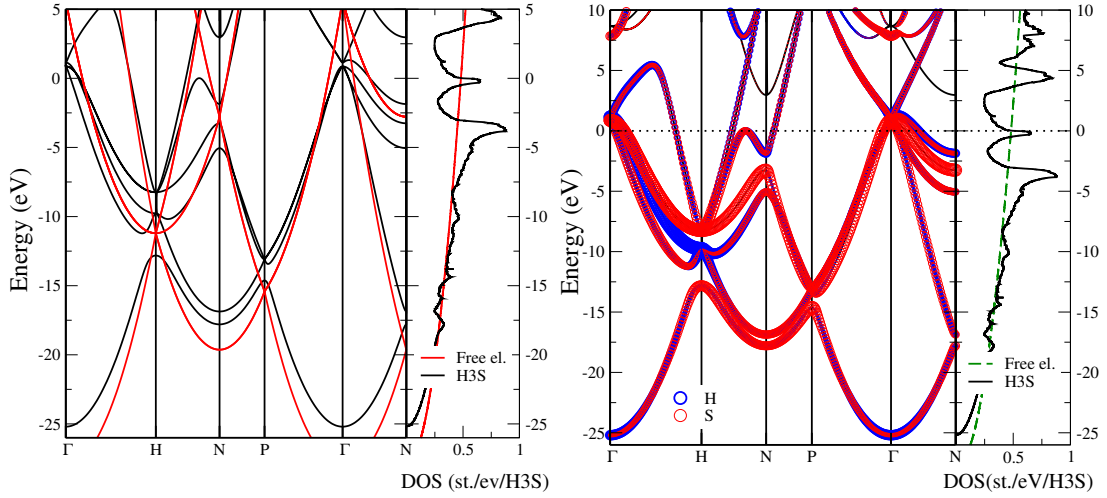


FIG. 6. Left: Free-electron bandstructure and density of states calculated for a bcc lattice with the same lattice parameter as H_3S at 200 GPa. The electronic structure and density of states of H_3S at 200 GPa are also shown for comparison. Right: Electronic structure of H_3S . The thickness of the band is proportional to the projection of the electronic state over a chosen atomic orbital (fat bands representation).

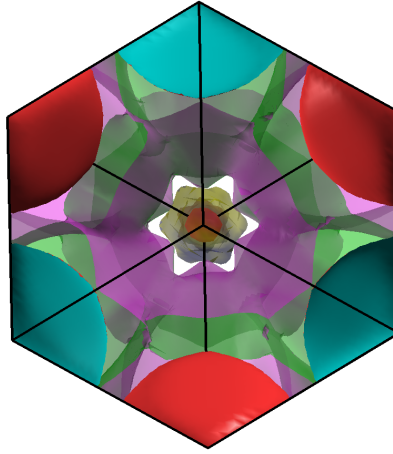


FIG. 7. Fermi surface of H_3S at 200 GPa including 5 sheets (right). The hole pockets at Γ are visible in the center. The large Fermi surface contributing most of the density of states is shown in transparent colors.

The Fermi surface is composed of 5 sheets. The avoided crossing at the zone center generates three hole pockets centered at Γ and a cubical electron Fermi surface centered at the N point. Finally, an additional large Fermi surface sheet arises from the electron-pocket at H.

Vibrational and superconducting properties of D_3S at 200 GPa

The phonon dispersion of D_3S calculated using harmonic linear response theory and the stochastic self-consistent harmonic approximation is shown in Fig. 8.

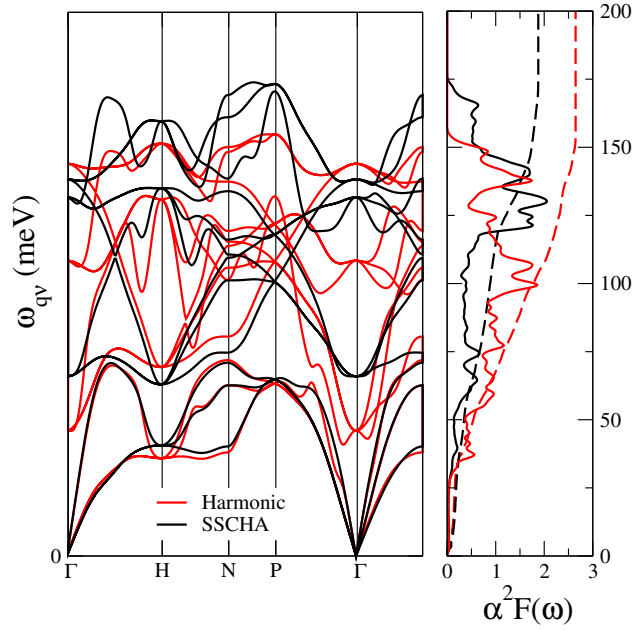


FIG. 8. Phonon spectrum, Eliashberg function and integrated electron-phonon coupling of D_3S at the harmonic and anharmonic levels (SSCHA).

Vibrational and superconducting properties of H_3S at 250 GPa

The phonon dispersion of D_3S calculated using harmonic linear response theory and the stochastic self-consistent harmonic approximation are shown in Fig. 9.

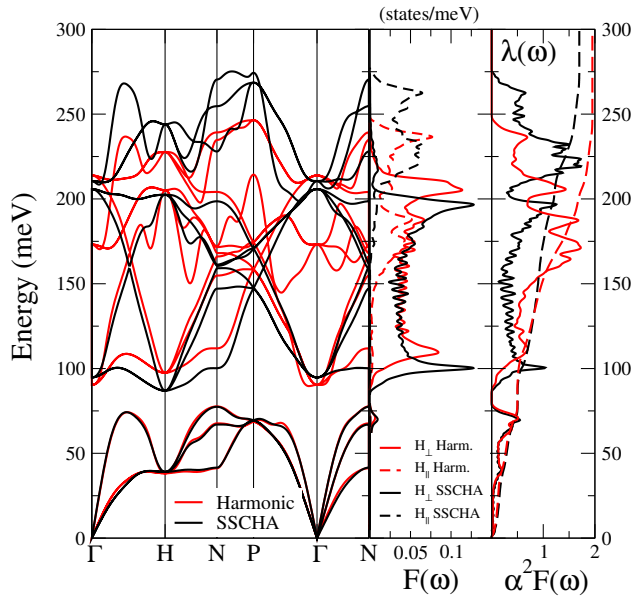


FIG. 9. Phonon spectrum, phonon density of states projected onto selected vibrations and the Eliashberg function and integrated electron-phonon coupling of H_3S at 250 GPa at the harmonic and anharmonic levels (SSCHA).

Migdal-Eliashberg

We solve the Isotropic Migdal-Eliashberg (ME) equations using either the harmonic Eliashberg function or the one calculated within the SSCHA. The equations are solved in the Matsubara frequency space using 512 Matsubara frequencies. The superconducting gap is obtained from the lowest Matsubara gap $\Delta_{n=0} = \Delta$ and is plotted in Fig. 10.

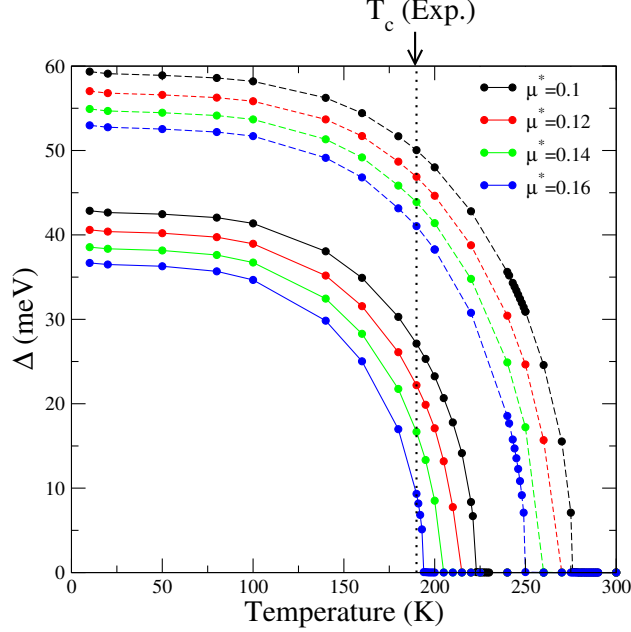


FIG. 10. Superconducting gap (Δ) as a function of temperature from the solution of the isotropic Migdal-Eliashberg equations applied to H_3S . The continuous lines refer to anharmonic phonon (SSCHA) while the harmonic phonon are denoted by dashed lines.

Superconducting properties using different approximations

TABLE IV. Electron-phonon interaction and a logarithmic average of phonon frequencies using the SSCHA, and without anharmonic effects. The T_c s are calculated using the SSCHA phonon spectrum and with either the McMillan equation (T_c^{MM}) or by solving the isotropic Migdal-Eliashberg equations (T_c^{ME}). A value of $\mu^* = 0.16$ is used.

Compound	λ^{har}	$\omega_{\text{log}}^{\text{har}}$ (meV)	λ^{anh}	$\omega_{\text{log}}^{\text{anh}}$ (meV)	$T_c^{\text{MM,har}}$	$T_c^{\text{MM,anh}}$	$T_c^{\text{ME,har}}$	$T_c^{\text{ME,anh}}$	$T_c(\text{Exp})$
H_3S (200 GPa)	2.64	90.4	1.84	92.86	158.8	124.9	250	194.0	190
H_3S (250 GPa)	1.96	109.1	1.71	101.3	155.25	127.2	226	190	
D_3S (200 GPa)	2.64	68.5	1.87	73.3	120.4	100.3	183	152.0	90

Effects of the vibrational energy on the pressure

In Fig. 11 the contribution of the atomic vibrations to the total energy is shown in the quasi-harmonic approximation and SSCHA. The ground state total energy, without the zero point energy (ZPE), is fitted to a second order polynomial as a function of the volume V , $E_0(V) = A_0 + B_0V + C_0V^2$. The fitting parameters are reported in Table V. We add the vibrational contribution to $E_0(V)$ calculated in the quasiharmonic approximation and in the SSCHA. This contribution is calculated at two volumes, those shown in the right panel of Fig. 11. The vibrational energy E_v is fitted linearly to $E_v(V) = A_v + B_vV$. As shown in Fig. 12, the linear fit provides a very good approximation to $E_v(V)$. The linear form of $E_v(V)$ is obtained within the quasiharmonic approximation for H_3S and D_3S , and in the SSCHA for H_3S . The ZPE energy is obtained using a $6 \times 6 \times 6$ phonon mesh.

The correction to the pressure from including the atomic vibrations is calculated from the $E(V) = E_0(V) + E_v(V)$ curves and $P(V) = -dE(V)/dV$. These curves are shown in Fig. 11. Neglecting the ZPE underestimates the pressure. The correction to the pressure from the ZPE is smaller for D_3S than for H_3S due to the smaller ZPE of deuterium. The SSCHA gives a small correction to the pressure obtained within the quasiharmonic approximation. The pressure corrections to the volumes for which the electron-phonon calculations were performed are summarized in Table VI.

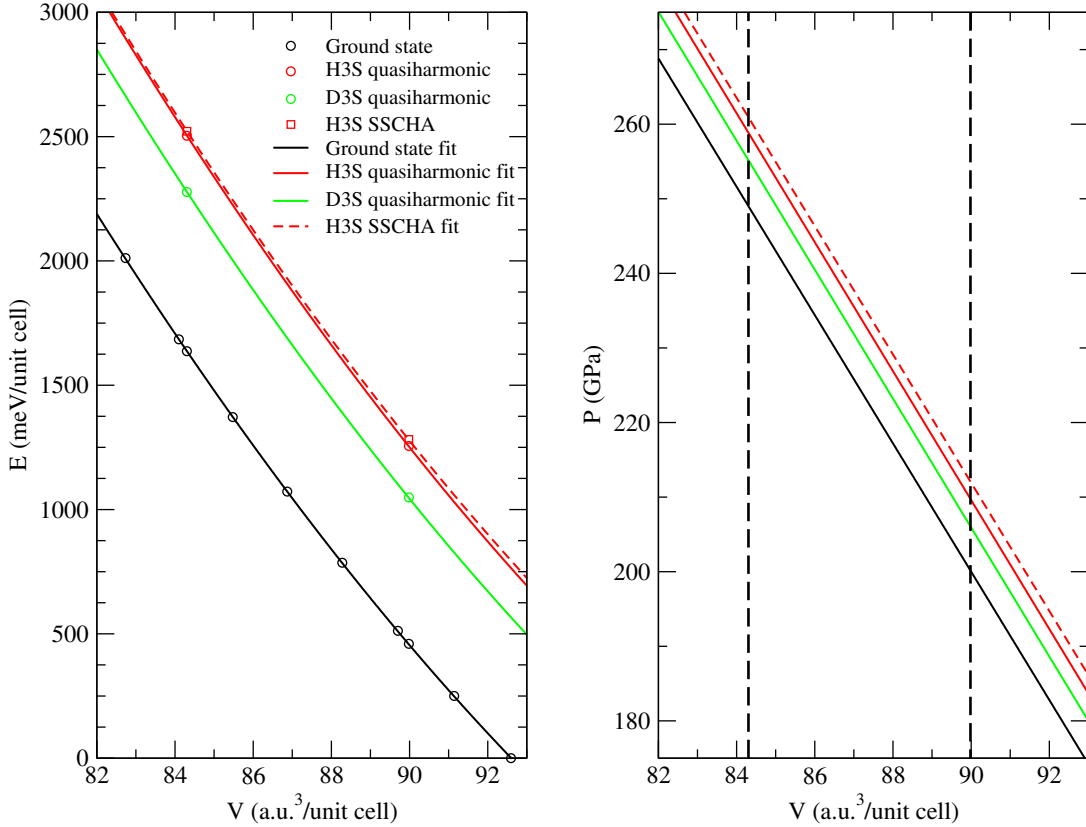


FIG. 11. (Left panel) Ground state energy without ZPE, including ZPE at the quasiharmonic level, and at the SSCHA level. The lines represent fitted curves following the recipe described in Sec. . (Right panel) The pressure derived from the fitted energy curves. The vertical dashed lines denote the volumes used in the SSCHA calculations.

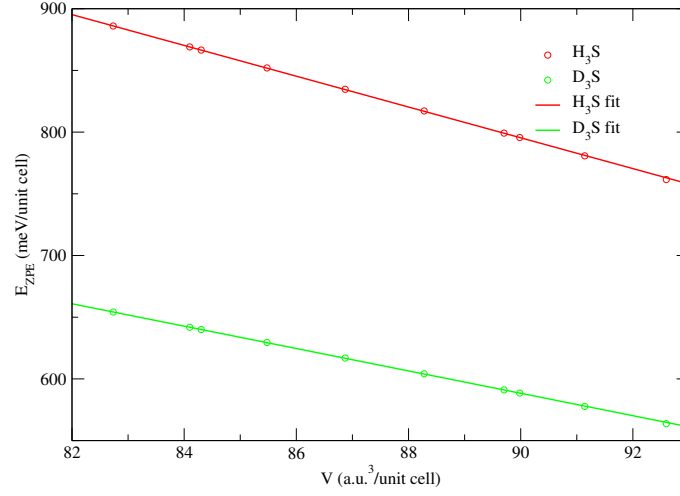


FIG. 12. ZPE calculated within the quasiharmonic level for H_3S and D_3S . The solid lines denote the linear fit obtained with two data points, the volumes are those from the right panel of Fig. 11.

TABLE V. Calculated parameters for the quadratic fit of $E_0(V)$ and the linear fit of $E_v(V)$.

	A_0 (mev)	B_0 (meV/a.u. ³)	C_0 (meV/a.u. ⁶)
	49319	-900.88	3.9772
	A_v (mev)	B_v (meV/a.u. ³)	
H_3S quasiharmonic	1918.5	-12.479	
D_3S quasiharmonic	1404.7	-9.0707	
H_3S SSCHA	1814.2	-11.027	

TABLE VI. Correction to the pressure P from the vibrational energy.

V (a.u. ³)	P (GPa)			
	no ZPE	D_3S quasiharmonic	H_3S quasiharmonic	H_3S SSCHA
89.9822	200	206	210	212
84.3035	250	255	259	261

* matteo.calandra@upmc.fr

- [1] J. P. Perdew, K. Burke, and M. Ernzerhof, Phys. Rev. Lett. **77**, 3865 (1996).
- [2] G. Kresse and J. Furthmüller, Comput. Mat. Sci. **6**, 15 (1996).
- [3] G. Kresse and J. Furthmüller, Phys. Rev. B **54**, 11169 (1996).
- [4] A. Togo, F. Oba, and I. Tanaka, Phys. Rev. B **78**, 134106 (2008).
- [5] C. J. Pickard and R. J. Needs, Nature Physics **3**, 473 (2007).
- [6] Olga Degtyareva, Eugene Gregoryanz, Maddury Somayazulu, Ho-kwang Mao, and Russell J. Hemley, Phys. Rev. B **71**, 214104 (2005).